Protoplasma (2015) 252:547–558
DOI 10.1007/s00709-014-0701-5

ORIGINAL ARTICLE

Modulation of liver and kidney toxicity by herb *Withania somnifera* for silver nanoparticles: a novel approach for harmonizing between safety and use of nanoparticles

Mohammad F. Anwar · Deepak Yadav · Shweta Rastogi · Indu Arora · Roop K. Khar · Jagdish Chander · Mohd Samim

Received: 29 April 2014 / Accepted: 10 September 2014 / Published online: 24 September 2014

Abstract In the present study, toxicity of nanoparticles is evaluated for assessing their effect on liver and kidney. We have synthesized highly mono-disperse spherical and rod-shaped silver nanoparticles using reverse microemulsion and aqueous phase methods. These were characterized by UV–vis spectrophotometer, dynamic light scattering, and transmission electron microscope confirming the formation of different sizes of spherical-shaped and rod-shaped silver nanoparticles (Ag NPs). Acute toxicity of different shapes and sizes of Ag NPs and their modulations by using *Withania somnifera* were evaluated through biochemical and histopathological changes in liver and kidney tissues of Wistar rats. We also evaluated cytotoxicity in specific murin macrophages through confocal microscopy. Cytotoxicity analysis indicates that median lethal dose (LD_{50}) for 20, 50, and 100-nm size spherical and 100-nm rod-shaped Ag NPs was 0.25, 0.35, 0.35, and 0.35 mg/ml, respectively. We also calculated clinically important protein concentration to illustrate the efficacy of Ag nanomaterials. These studies indicated that 20, 50, and 100-nm spherical Ag NPs (35 mg/kg, 23 days) increased the biochemically important enzymes and substrate levels glutamate oxaloacetate transaminase (GOT), glutamate pyruvate transaminase (GPT), alkaline phosphatase (ALP), creatinine, and urea concentration in serum, showing liver and kidney tissue damage. After 23 days of treatment of Ag NPs (20, 50, and 100 nm spherical), along with *W. somnifera*, toxicity of Ag NPs significantly decreased and marginalized. However, no significant changes were observed for 100-nm rod-shaped Ag NPs on normal liver and kidney architecture. Given their low toxic effects and high uptake efficiency, these have a promising potential as to lower the toxicity of Ag NPs.

Keywords Silver nanoparticles · Oral acute toxicity · Confocal microscopy · Cytotoxicity · In vivo · *Withania somnifera*

Abbreviations

SGOT	Serum glutamic oxaloacetic transaminase
SGPT	Serum glutamic pyruvic transaminase
ALP	Alkaline phosphatase
BUN	Blood urea nitrogen
TEM	Transmission electron microscopy
MTT	3-(4,5-Dimethylthiazol-2-yl)-2,5-diphenyltetrazolium bromide
Ag NPs	Silver nanoparticles
LD_{50}	Median lethal dose

Handling Editor: Reimer Stick

Electronic supplementary material The online version of this article (doi:10.1007/s00709-014-0701-5) contains supplementary material, which is available to authorized users.

M. F. Anwar · S. Rastogi · M. Samim
Department of Chemistry, Faculty of science, Hamdard University, New Delhi 110062, India

D. Yadav
Faculty of Medicine, Hamdard University, New Delhi 110062, India

R. K. Khar
Department of Pharmacy, B.S. Anangpuria Institute of Health Sciences, Faridabad, Haryana, India

J. Chander
Department of Science and Technology, Technology Bhawan, New Delhi 110016, India

I. Arora
Department of Biomedical Sciences, Shaeed Rajguru College of Applied Sciences, University of Delhi, Vasundhra Enclave, New Delhi 110095, India

M. Samim (✉)
Department of Chemistry, Faculty of Science, Jamia Hamdard, Hamdard Nagar, New Delhi 110062, India
e-mail: samimnano@gmail.com

DLS Dynamic light scattering
AOT Sodium bis(2-ethylhexyl) sulfosuccinate
EDTA Ethylenediaminetetracetic acid

Introduction

Withania somnifera (L) Dunal, commonly known as Ashwagandha, is a perennial medicinal herb belonging to the order Solanaceae and, from ancient times, widely used in Ayurvedic medicine as a tonic to rejuvenate the body and prevent diseases (Kumar et al. 2011; Sharma et al. 2011). The biologically active chemical constituents of *W. somnifera* are alkaloids (isopellertierine, anferine), steroidal lactones (withanolides, withaferins), saponins (sitoindoside VII and VIII), withanolides (sitonidoside XI and X), and iron (Budhiraja et al. 1987; Niyaz and Siddiqui 2014). *W. somnifera* has extensive pharmacological activities in the field of traditional medicinal system and used as anti-tumor (Oberpichler et al. 1990), anti-inflammatory (Nittala and Lavie 1988), immunity stimulator (Kandil et al. 1994), anti-depressant (Abou-Douh 2002), anti-aging (Wagner et al. 1994), and anti-oxidant activities (Singh et al. 2003; Bhattacharya et al. 2001; Dhalla et al. 1961). In other reports, *W. somnifera* has also shown anti-osteoarthritic (Kulkarni et al. 1991) and anti-stroke activities (Chaudhary et al. 2003). Its two compounds, sitoindosides VII–X and withaferin A (glycowithanolides), have been studied for anti-oxidant activities which act with the help of free radical scavenging enzymes, superoxide dismutase (SOD), catalase (CAT), and glutathione peroxidase (GPX) (Panda and Kar 1997). Therefore, in the present study, *W. somnifera* was used to evaluate the change in the toxicity created by silver nanoparticles into the liver and kidney tissues.

There are several reports stating that silver nanoparticles (Ag NPs) have wide application for human uses. Hence, the toxicity studies of Ag NPs become a topic of important research. Researchers are focused on procedures used for the production of size and shaped-controlled of Ag NPs due to their distinct properties and potential use in various fields such as anti-microbial, optical, electromagnetic, catalytic properties, and other biological characteristics in comparisons of bulk silver (Wagner et al. 1994; Alarco et al. 2012; Choi et al. 2009). The anti-microbial properties of Ag NPs are being evaluated for their use in daily household products like washing machines; water purification; toothpaste; shampoos; and disinfecting bedding, nipples, nursing bottles, fabrics, deodorants, filters, kitchen utensils, toys, and humidifiers etc. (Anwar et al. 2013; Cheng et al. 2004; Lankveld et al. 2010; Ahamed et al. 2010). Ag NPs also have been found application in surgical instruments as well for in wound dressings and contraceptive devices (Muangman et al. 2006; Cohen et al. 2007; Lansdown 2006; Zhang and Sun 2007; Lu et al. 2010). The differences in shape and size of Ag NPs are being controlled with the help of reducing agent, stabilizer, and various methods (He et al. 2004; Wang et al. 2005).

Ag NPs have toxicity due to their size, structure, shape, and chemical–physical environment (Carlson et al. 2008; Park et al. 2011; Huiliang et al. 2011; Nel et al. 2012). As utilization of Ag NPs is continuously expanding, the risks regarding the health implications due to lack of information on the basic toxicity of size and shape dependence of Ag NPs are enormous (Yong et al. 2010). Therefore, the objective of this study was designed to investigate the acute toxicity effects associated with various sizes and shape of Ag NPs and its toxicity modulation by *W. somnifera*. Considering the applications of *W. somnifera*, it was used as herbal remedy to reduce the toxic effect of various Ag NPs in vivo model on Wistar rats. Before conducting in vivo study, we evaluate the adverse effect of Ag NPs against murin macrophages using 3-(4,5-dimethylthiazol-2-yl)-2,5-diphenyltetrazolium bromide (MTT) assay.

Materials and methods

Materials

Aerosol OT (AOT; sodium, bis(2-ethylhexyl) sulfosuccinate), hexane, silver nitrate ($AgNO_3$), tri-sodium citrate, sodium borohydride ($NaBH_4$), ascorbic acid, and aqueous solution of hydrazine were purchased from Sigma-Aldrich, USA. Roswell Park Memorial Institute (RPMI) 1640 and MTT were purchased from Merck, India. Glutamate oxaloacetate transaminase (GOT), glutamate pyruvate transaminase (GPT), alkaline phosphatase (ALP), creatinine, and blood urea nitrogen (BUN) assay kits were purchased from Span Diagnostic Pvt. Ltd., Surat, India. *W. somnifera* was procured from Green Earth Products Pvt Ltd, India.

Methodology

Synthesis of spherical-shaped silver nanoparticles by microemulsion method

Reverse micelles of AOT were prepared by dissolving 0.444 g AOT in 10 ml hexane and adding precise volumes of water containing metal precursor or hydrazine. The amount of solubilized water is usually expressed as a molar ratio of water to AOT, i.e., $W_0=[H_2O]/[AOT]$. For preparation of Ag NPs, 75 μl of 0.1, 1.5, and 0.2-M aqueous solution of silver nitrate was added to 5 ml 0.1-M AOT solution. The resulting solution was stirred for 6 h on magnetic stirrer to form microemulsion (A). In another set of reaction, 75 μl (0.3 M), 75 μl (0.45 M), and 75 μl (0.6 M) of hydrazine hydrate solution were added drop wise to 5-ml AOT (0.1 M) solution. Similarly, this

solution was also stirred for 6 h on magnetic stirrer to form microemulsion, named B. The molar ratio of hydrazine hydrate and silver nitrate was held constant for all experiment at a value of 3. In order to reduce the silver ions, microemulsion (B) containing hydrazine hydrate was added slowly into microemulsion (A) containing silver nitrate drop by drop and was subjected to continuous stirring for 6 h. Subsequently, the color of the microemulsion changed from colorless to a yellowish brown color, indicating the formation of spherical-shaped Ag NPs.

Synthesis of rod-shaped silver nanoparticles by aqueous-phase method

Aqueous solution of 2×10^{-4} M silver nitrate and anhydrous solution of 1×10^{-3} M sodium bis(2-ethylhexyl) sulfosuccinate (AOT) in hexane were prepared. In 100 ml of round bottom flask, 50 ml of silver nitrate solution and 35 μl of anhydrous AOT solution were mixed by stirring for 1 h. Six hundred-microliter aqueous solution of 1×10^{-2} M tri-sodium citrate was added to the above solution and was refluxed at 100 °C with constant stirring for 70 min. After refluxing, reaction mixture becomes turbid and turns yellow-green. The final reaction mixture contained both spherical as well as rod-shaped Ag NPs. The silver nanorods were separated from the spherical particles by centrifuging the sample at 2,000 rpm for 30 min at 25 °C. The silver nanorod settled at the bottom of their container after centrifugation. The AOT and spherical-shaped Ag NPs were removed using a pipette. This separation procedure was repeated several times until the supernatant becomes colorless.

Characterization of Ag nanoparticles

UV–vis spectroscopy

UV–vis absorption spectra (UV-1601 Shimadzu, Japan) were use to find characteristic plasma band of the Ag nanoparticles.

Dynamic light scattering

Dynamic light scattering was used to determine the size distribution profile of small particles in suspension solution (Malvern Zetasizer ver. 6.01) at 25 °C with light scattering at 90° in the aqueous and nonaqueous medium.

High-resolution transmission electron microscopy

Field-emission transmission electron microscope (FE-TEM) [JEOL, JEM-2100, and 200 kV] was used for analysis. Samples were prepared by placing small drops of aqueous dispersions lyophilized Ag NPs on carbon-coated copper grids and allowing the solvent to slowly evaporate at room temperature.

3-(4,5-Dimethylthiazol-2-yl)-2,5-diphenyltetrazolium bromide assay

Macrophages were collected by peritoneal lavage from sodium thioglycolate-stimulated mice. The peritoneal cells were collected in RPMI 1640 medium (incomplete), centrifuged at 1,400×*g* for 10 min at 4 °C, washed twice, and finally resuspended in complete medium. Macrophages at a density of 1×10^{6} cells ml^{-1} were seeded in 96-well tissue culture plates (0.1 ml per well) and exposed to various sizes of Ag NPs (20, 50, and 100 nm spherical shape and 100 nm rod shape) at a concentration of 5, 15, 25, and 35 μg/ml for 12 h in a CO_2 incubator (5 % CO_2, 37 °C) to calculate the median lethal dose (LD_{50}). Cell viability was evaluated using a modified MTT assay, where the conversion of MTT to formazan by mitochondrial enzymes served as an indicator of cell viability and amount of dye produced is directly proportional to the number of metabolically active cells (24) Accordingly, absorbance at 492 nm represented the number of live cells. LD_{50} value was calculated from the dose–response curve and used as a measure for drug resistance, and the mean percentage viability was calculated as follows:

$$\frac{\text{Mean specific absorbance of treated macrophages}}{\text{Mean specific absorbance of untreated macrophages}}\times 100$$

Cellular uptake of Ag NPs

Cellular uptakes of Ag NPs (20, 50, and 100 nm spherical shape and 100 nm rod shape) after 4-h incubation in microphages obtained from peritoneal lavage were visualized in TCS-SPE confocal laser scanning microscopy, equipped with an DMI4000 microscope (Leica Microsystems CMS GmbH, Germany) with a ×40 objective and 532-nm wavelength of laser radiation class 3B at scanning speed 800 Hz. LAS-AF software (Leica Microsystems) was used for data acquisition and processing.

In vivo study

Animals

Forty-five healthy Wistar albino rats of 7 to 8 weeks age, each weighing 250–350 g, were obtained and maintained in the Animal House of the Jamia Hamdard, New Delhi. They were kept under 12-h light–dark cycle at a temperature 24±1 °C and relative humidity 55±10 % and were acclimatized for 1 week prior to the experiment with animal feed (Hindustan Pvt. Ltd., India) and water supplied ad libitum. All animal experiments were performed according to the procedures

established by the Ethical Committee of Jamia Hamdard, New Delhi, India (CPCSEA/173).

*Preparation of the **W. somnifera** root extract*

Approximately, 1 g of dried powder of *W. somnifera* root is poured into a 500-ml Erlenmeyer flask with 100 ml triple-distilled water, and the solution was kept overnight; then, the mixture was boiled up to one fourth of its volume. The solution is cooled at room temperature and finally filtered with Whatman filter paper to obtain a light-brown-colored aqueous extract of the *W. somnifera* root.

The obtained extract was further concentrated under vacuum to dry form. The residue obtained was then redissolved in water to the desired final concentration of 50 mg/kg body weight of *W. somnifera*.

*Acute toxicity and treatment with **W. somnifera***

The acute toxicity of Ag nanoparticles on rats was examined following the protocol of Yong et al. 2010. Forty-five healthy rats were divided randomly into nine groups designated as groups 1–9, with each group comprising five rats. Rats in group 1 were given saline orally for 23 days daily and used as a control. Groups 2, 3, and 4 were administered 20, 50, and 100-nm spherical-shaped Ag NPs, respectively, whereas group 5 was given 100-nm rod-shaped Ag NPs. Fixed concentration of 35 mg/kg doses was given orally to groups 2–5 to evaluate acute toxicity in rats. Groups 6–9 were administered 35 mg/kg doses of Ag NPs (20, 50, and 100 nm spherical shape, and 100 nm rod shape, respectively) with *W. somnifera* (35 mg/kg BW) for 23 days to examine modulated toxicity.

Biochemical analysis

Blood samples were collected from cardiac puncture of rats into clean dry bottles containing ethylenediaminetetracetic acid (EDTA). Plasma was separated by centrifugation at 3,000 rpm for 5 min and stored at −20 °C until analysis for biochemical parameters. GOT, GPT (Reitman and Frankel 1957), and ALP (King and King 1954) activities were determined in plasma at 570, 340, and 405 nm, respectively, by UV–vis spectrophotometer according to the method described by Kind and King's. Creatinine and urea concentrations were determined at 490 and 340 nm following the Husdan and Rapoport method (Husdan and Rapoport 1968), and urease and Berthlot method (Allain et al. 1978), respectively.

Histopathological examination

Ag NP-treated groups were compared with control group to observe liver and kidney tissue histopathology. On the last day of experiment, rats were anesthetized with ether and were perfuse transcardinally with saline. Samples of the liver and kidney were removed, postfixed in 10 % neutral buffered formalin for 24 h and processed for histopathological examinations (Wang et al. 2005). After fixation, 3–4-mm slices of tissues were dehydrated and embedded in paraffin. Cross sections of 5-μm thickness were cut washed with xylene, and tissues were mounted with DPX. Hematoxylin and eosin (H and E) stains were used to visualize and differentiate between normal tissue and Ag NP-treated tissues, and microphotographs were taken using an Olympus BX50 microscope (Olympus, Japan).

Statistical analysis

Cytotoxicity data was fitted in a parameter nonlinear logistic model from add-on options in Microsoft Excel, to calculate the lethal dose of Ag NPs that caused a 50 % inhibition in comparison with untreated controls. All LD_{50} values were calculated using the average cytotoxicity data of the three independent experimental results along with their associated errors, and the values are reported in ±95 % confidence intervals (±95 % CI) for the triplicate set of each experimental condition. Data are represented as mean±standard deviation (SD), and statistical analysis were carried out to know the variance of results using ANOVA analysis followed by Dunnett's test.

Results

Characterization of Ag nanoparticles

Dynamic light scattering analysis

Dynamic light scattering is a technique in physics which can be used to determine the size distribution profile of small particles in suspension. The hydrodynamic diameters (d) of Ag NPs were calculated by using the Stokes–Einstein equation $d = k_B T / 3\pi\eta D$, where k_B is the Boltzmann constant, T is the absolute temperature, η is the solvent viscosity, and D is the diffusion coefficient. CONTIN algorithms were used in the Laplace inversion of the autocorrelation function to obtain the size distribution (Wilhelm et al. 1991). The number average mean hydrodynamic sizes of Ag NPs at W_0 corresponding to 10, 12.5, and 15 were 20.21, 50.21, and 100 nm (Supporting Information Fig. S1a–c), respectively, with a narrow polydispersity index (0.22–0.29).

UV–vis spectrophotometer analysis

The UV–vis spectra of the synthesized spherical-shaped and rod-shaped Ag NPs are given in Supporting Information Fig. S2. The spectra illustrate that with increasing water

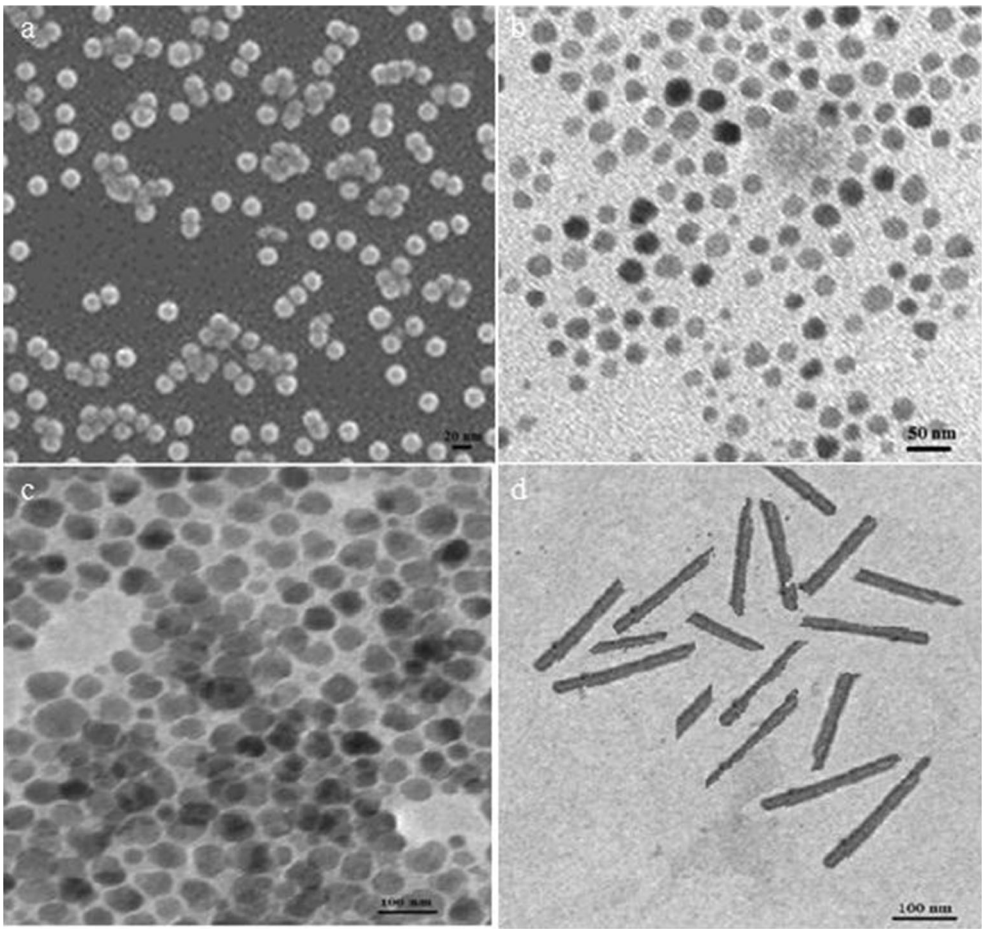

Fig. 1 HR-TEM micrograph of **a** 20 nm at 75 μl silver salt, **b** 50 nm at 100 μl silver salt, and **c** 100 nm at 150 μl silver salt with spherical shape synthesized through AOT microemulsion and **d** HR-TEM micrograph of 100-nm rod-shaped silver nanoparticles

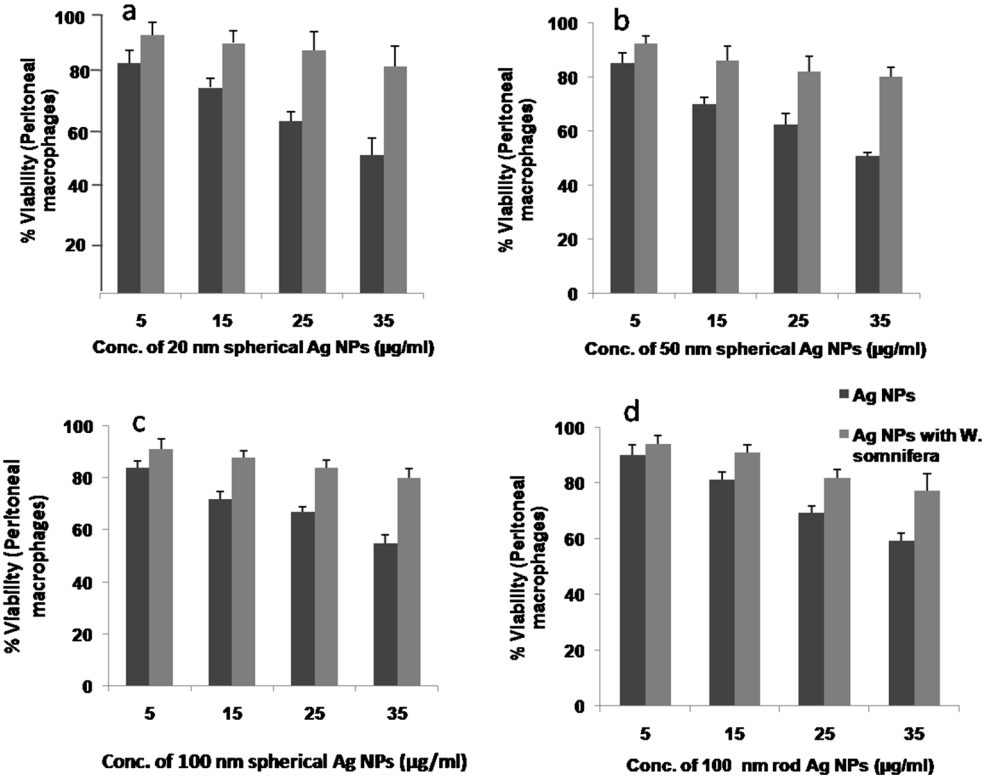

Fig. 2 Plots of cell viability MTT assay studied for Ag NPs after 12-h incubation period at different doses (5, 15, 25, and 35 μg/ml). **a** 20-nm spherical-shaped Ag NPs treated showing more toxic. **b** 50-nm spherical-shaped Ag NPs treated. **c** 100-nm spherical-shaped Ag NPs treated. **d** 100-nm rod-shaped Ag NPs treated

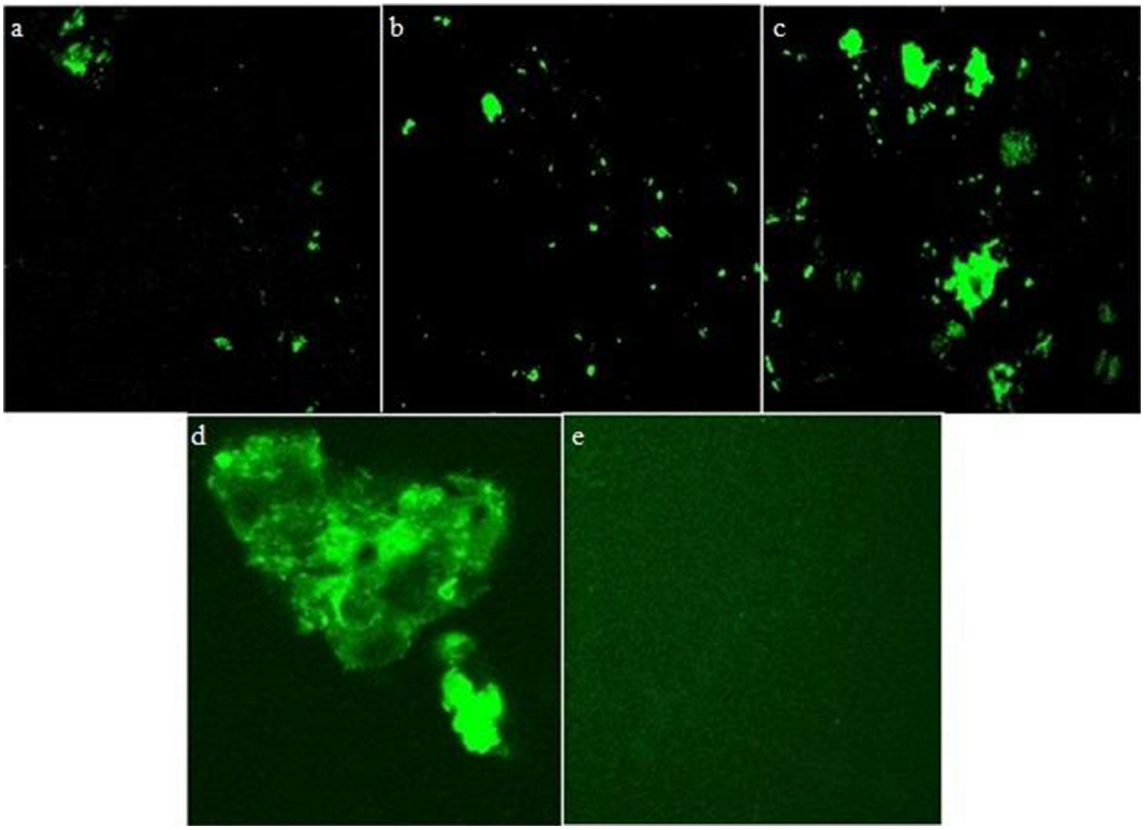

Fig. 3 Cellular uptake of Ag NPs in macrophages obtained from murin peritoneal lavage after 4-h incubation at 37 °C. Cellular uptake was determined by confocal microscopy. **a** 100-nm spherical-shaped Ag NPs, **b** 50-nm spherical-shaped Ag NPs, **c** 20-nm spherical-shaped Ag NPs, **d** 100-nm rod-shaped Ag NPs, and **e** control without nanoparticles

contents in microemulsion, core size microemulsion increased and formed bigger nanoparticles than that with lower water contents, and accordingly, a red shift in plasma band of Ag NPs was observed. The absorption spectra were recorded at 407, 423, and 429 nm for Ag NPs synthesized at water content W_0 10, 12.5, and 15, respectively. The silver nanorods showed

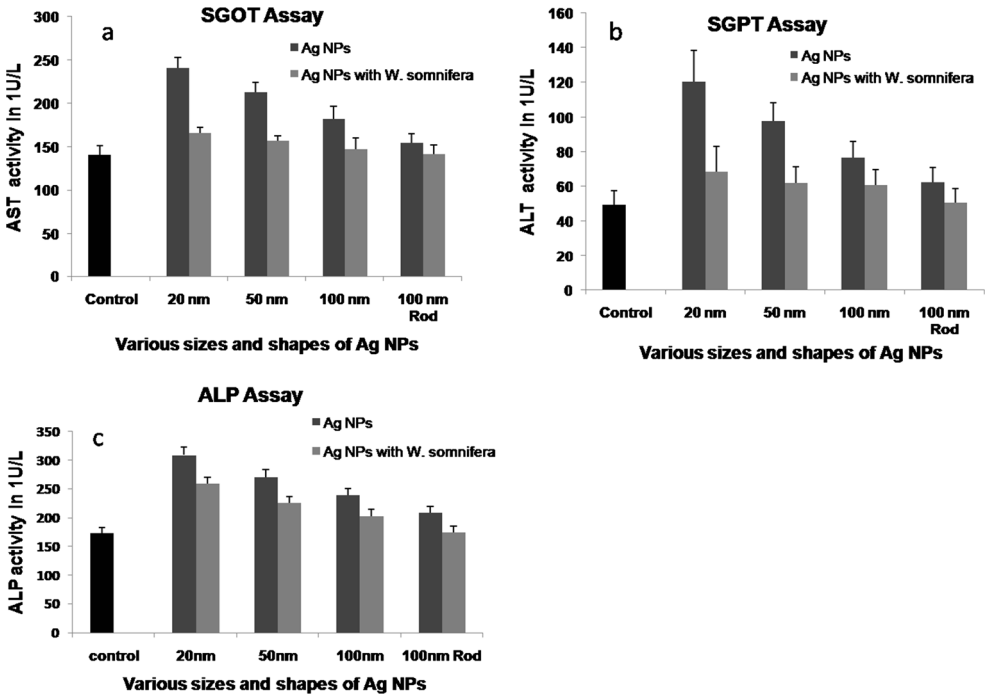

Fig. 4 **a**–**c** Shows increased level of SGOT, SGPT, and ALP, respectively, for 20, 50, and 100-nm spherical Ag NPs, while for 100-nm rod Ag NPs, there is a slightly change in SGOT level. When rats are treated with AgNPs and *W. somnifera*, together it reduced significantly the SGOT, SGPT, and ALP levels

two plasma bands in absorption spectrum at 584 nm due to transverse plasmon band and the other at 435 nm due to longitudinal plasmon band. This confirmed that we were able to synthesize rod-shaped Ag nanomaterials from second synthetic route.

High-resolution transmission electron microscope analysis

The average sizes of Ag NPs synthesized by microemulsion synthesis route were calculated from HR-TEM image as 20, 50, and 100 nm at 10, 12.5, and 15 W_0 (Fig. 1a–c), all having spherical shape. The second route generated rod-shaped nanoparticles as seen from TEM image (Fig. 1d) which were in correlation with data from both dynamic light scattering (DLS) and UV–vis spectra.

Toxicity analysis

MTT assay

A dose-dependent response was observed in MTT assay for calculating LD_{50} values, and cytotoxicity data for Ag NPs and macrophages is presented in Fig. 2a–d. LD_{50} values for 20-nm Ag NPs were the most sensitive among all nanoparticles (Fig. 2a) in macrophages. One hundred-nanometer rod-shaped Ag NPs (Fig. 2d) were found to be least sensitive in macrophages, while 100-nm spherical-shaped Ag NPs were found to be more toxic. Cell viability was found to decrease with the decreasing size of Ag NPs and exposure time in macrophages. However, viability was always above than 80 % for treated groups with *W. somnifera* (23 days) and various sizes and shapes of Ag NPs (Fig. 2).

LD_{50} values of 20-nm Ag NPs are much lower than those of 100-nm spherical Ag NPs at all exposure time points which has slightly higher values as compared to 100-nm rod-shaped Ag NPs after 12 h of exposure time. The LD_{50} values were 0.25 mg/ml (confidence interval ±2.97), 0.35 mg/ml (confidence interval ±1.09), 0.35 mg/ml (confidence interval ±1.09), and 0.35 mg/ml (confidence interval ±1.09) for 20, 50, and 100-nm spherical-shaped Ag NPs and 100-nm rod-shaped Ag NPs, respectively. This shows that the small-sized Ag NPs have much cytotoxicity in comparison with 100-nm Ag NPs, and 100-nm rod-shaped Ag NPs have least toxicity in comparison with spherical-shaped Ag NPs.

Cellular uptake of Ag NPs

Confocal laser scanning microphotographs of cell containing Ag NPs were taken, and the diameter of diffraction-limited spot corresponds to $d_B = 1.22 * \ddot{e}/NA$, with $\ddot{e}$ representing the excitation wavelength and NA numerical aperture of the objective used with illuminations of specimens that are focused on the smallest possible spot. After 4-h exposure, 20, 50, and 100-nm spherical-shaped and 100-nm rod-shaped Ag NPs were visualized together with control without nanoparticles (Fig. 3a–e). These analyses showed that high cellular uptake in macrophages was obtained from murin peritoneal lavage after 4-h incubation at 37 °C. With decreasing size of Ag NPs, there had been rapid penetration in the cells that were dying out of the population (Liu et al. 2013).

Biochemical analysis

Results of biochemical assay showed that serum glutamic oxaloacetic transaminase (SGOT), serum glutamic pyruvic transaminase (SGPT), and ALP levels increased with 20, 50, and 100-nm Ag spherical NP-treated Wistar rats in comparison with control group. On the other hand, 100-nm rod Ag NP-treated rats had slightly increased SGOT levels, and no changes in SGPT and ALP levels were observed. Wistar rats treated with Ag NPs along with *W. somnifera* significantly

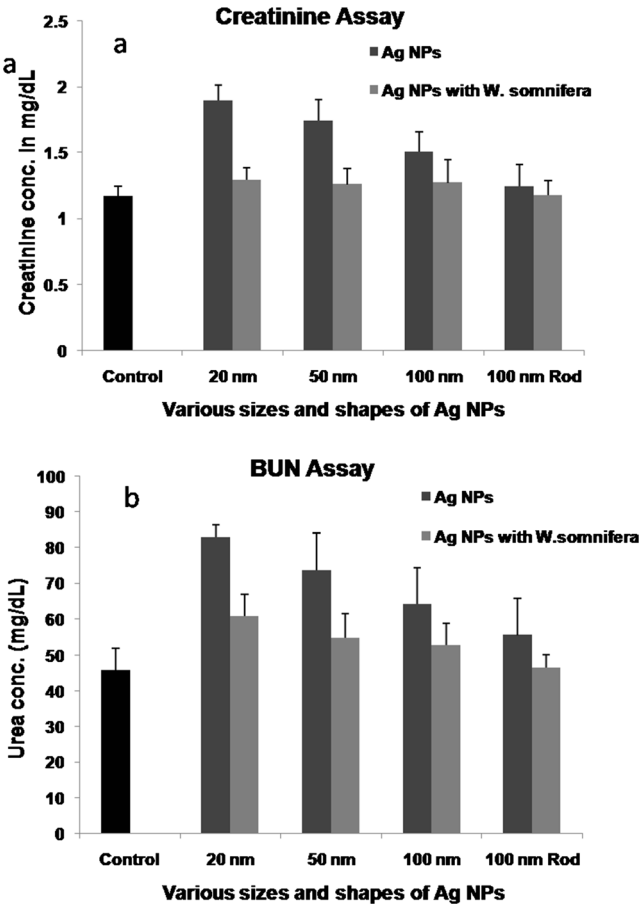

Fig. 5 **a** Graph showing that only 20-nm Ag NPs slightly increased the creatinine, while 50/100-nm (spherical) and 100-nm Ag NPs (rod) and Ag NPs with *W. somnifera*-treated groups have no effect on creatinine concentration. **b** Graph showing that 20, 50, and 100-nm Ag NPs (spherical) increased the BUN level while Ag NPs (rod 100 nm) slightly changed the BUN level. When rats are treated with Ag NPs and *W. somnifera*, together it reduced the BUN level

reduced SGOT, SGPT, and ALP levels in control group (Fig. 4a–c). Creatinine values were increased only for 20-nm Ag NPs while no changes were observed for 50 or 100 nm (spherical) and rod 100-nm Ag NPs alone and with *W. somnifera*-treated groups (Fig. 5a). Spherical-shaped 20, 50, and 100-nm Ag NPs increased the BUN level. In rats treated with Ag NPs, along with *W. somnifera*, the BUN level reduced to normal level as in control group (Fig. 5b).

Histopathological examination

Photomicrographs of liver and kidney tissues showed histopathological changes in liver tissue on treatment with Ag NPs and are illustrated in Fig. 6. Control group showed normal liver architecture, portal triad (PT), and central vein (CV) whereas 20-nm Ag NP-treated animal showed vacuolation of hepatocytes, focal necrosis in the centrizonal area, inflammation, and dilated CV. Animals treated with 50-nm Ag NPs have moderate sinusoidal dilatation in the centrizonal area and no necrosis, and hepatocytic vacuolation has been seen in portal triad (Fig. 6c). One hundred-nanometer spherical and 100-nm rod Ag NPs showed sinusoidal dilatation in the centrizonal area, dilated CV, and moderate sinusoidal dilatation in the centrizonal area, and normal PT and CV, respectively (Fig. 6d, e). *W. somnifera* resulted in reduced toxicity of 20, 50, and 100-nm Ag NPs as depicted with mild vacuolation in centrizonal area and dilated CV and PT, large vacuolation of hepatocytes in centrizonal area, inflammation with intact CV, mild vacuolation, and normal PT and CV, respectively (Fig. 6f–h). Rod-shaped 100-nm Ag NPs with *W. somnifera* showed normal liver architecture with PT and CV (Fig. 6i).

Histopathological changes in kidney tissue were also examined; control group showed normal kidney architecture with glomerula and normal cells, and treated groups by 20-nm Ag NPs showed nuclear loss, karyolysis, hyalinization, glomerular destruction, and necrosis and by 50-nm Ag NPs,

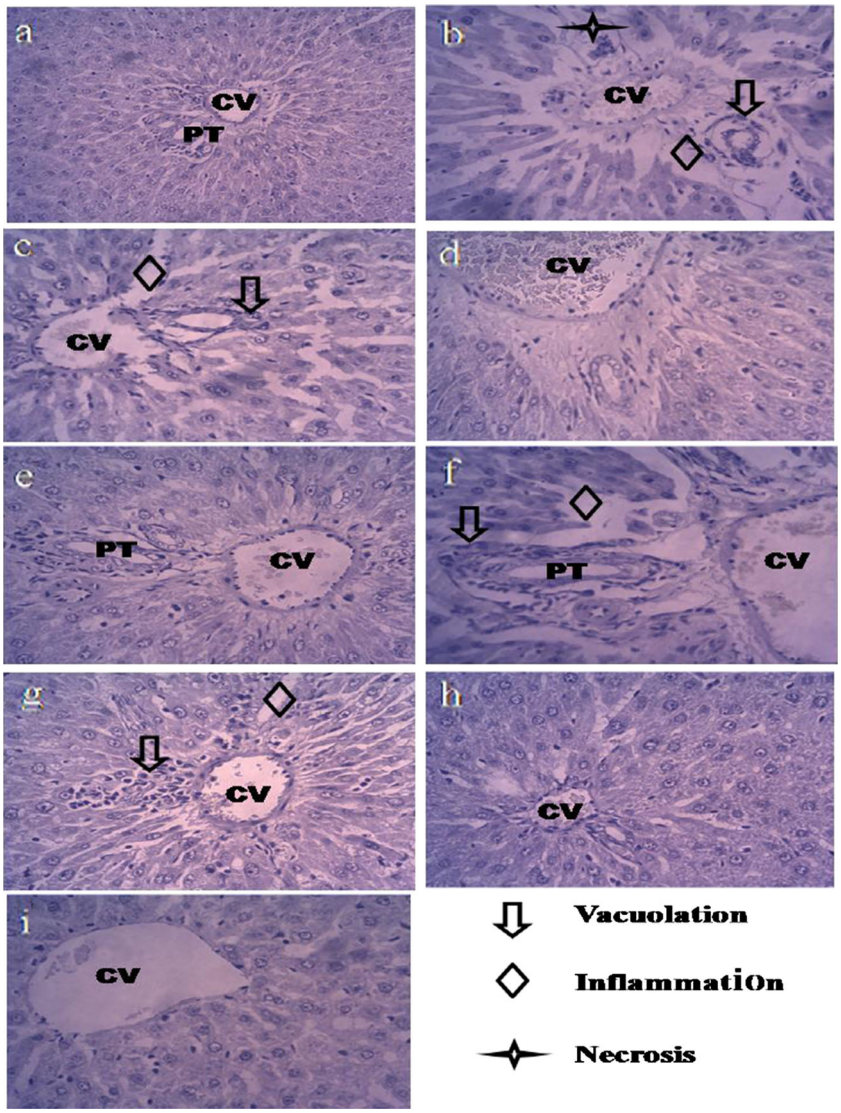

Fig. 6 Photomicrographs showing histopathological changes in liver tissue. **a** Control group (×40) showing normal liver architecture, portal triad (*PT*), and central vein (*CV*). **b** Treated group (20-nm Ag NPs) (×40) showing vacuolation of hepatocytes and focal necrosis in the centrizonal area and inflammation and dilated CV. **c** Treated group (50-nm Ag NPs) (×40) showing moderate sinusoidal dilatation in the centrizonal area and no necrosis, and hepatocytic vacuolation is seen PT. **d** Treated group (100-nm Ag NPs) (×40) showing sinusoidal dilatation in the centrizonal area and dilated CV. **e** Treated group (rod 100-nm Ag NPs) (×40) showing moderate sinusoidal dilatation in the centrizonal area and normal *PT* and CV. **f** Treated group (20-nm Ag NPs with *W. somnifera*) (×40) showing mild vacuolation in the centrizonal area and dilated CV and *PT*. **g** Treated group (50-nm Ag NPs with *W. somnifera*) (×40) showing large vacuolation of hepatocytes in centrizonal area and inflammation with intact CV. **h** Treated group (Ag NPs 100 nm with *W. somnifera*) (×40) showing mild vacuolation and normal PT and CV. **i** Treated group (rod 100-nm Ag NPs with *W. somnifera*) (×40) showing normal liver architecture with PT and CV

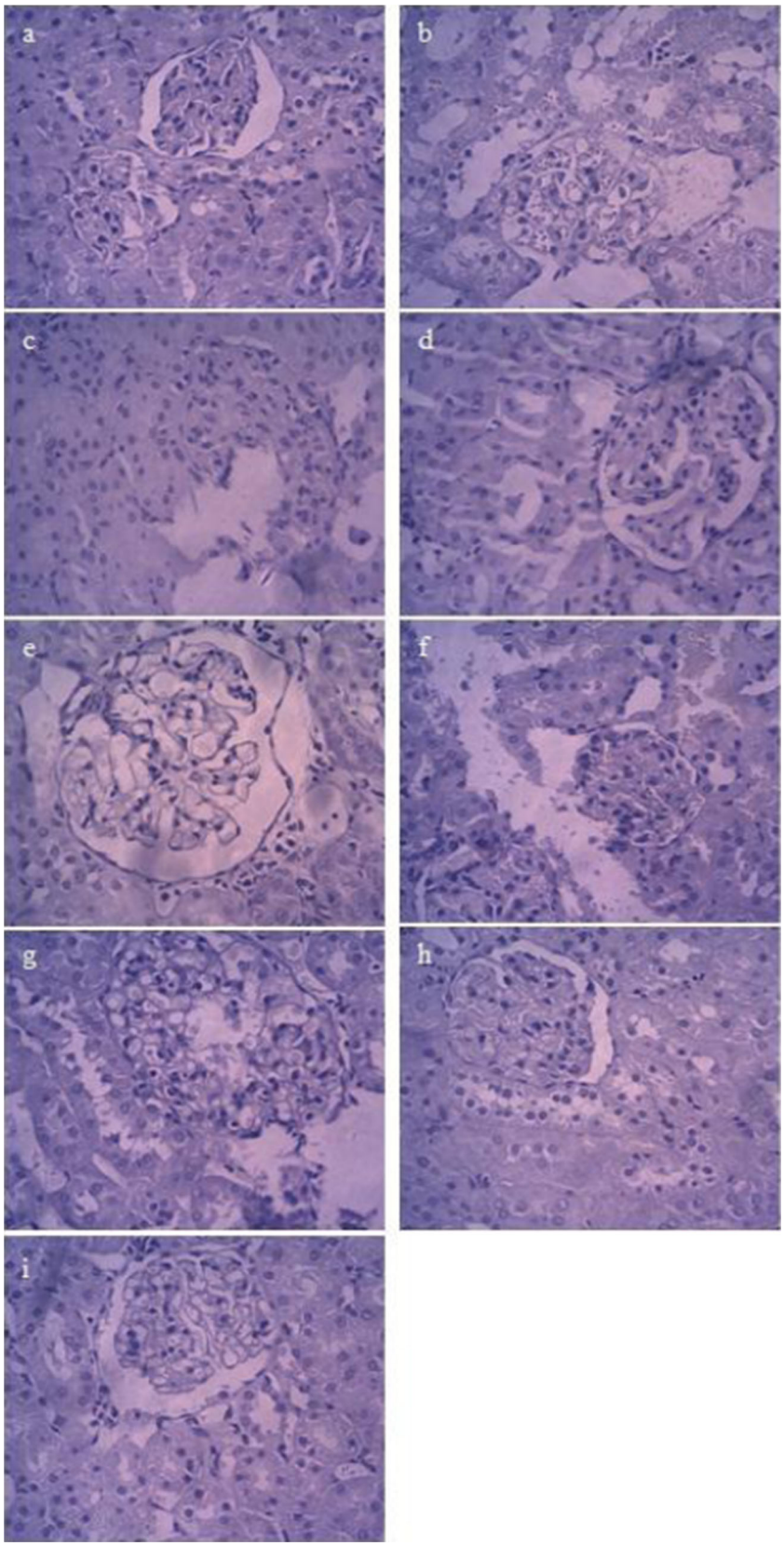

Fig. 7 Photomicrographs showing histopathological changes in kidney tissue. **a** Control group (×40) showing normal kidney architecture with glomerula and normal cells. **b** Treated group (20-nm Ag NPs) (×40) showing nuclear loss, karyolysis, hyalinization, glomerular destruction, and necrosis. **c** Treated group (50-nm Ag NPs) (×40) showing mild hyalinization, eosinophilia, and mild glomerular destruction. **d** Treated group (100-nm Ag NPs) (×40) showing normal glomerula and mild hyalinization. **e** Treated group (rod 100-nm Ag NPs) (×40) showing normal glomerula and mild hyalinization. **f** Treated group (20-nm Ag NPs with *W. somnifera*) (×40) showing hyalinization, eosinophilia, mild glomerular destruction, and no necrosis. **g** Treated group (50-nm Ag NPs with *W. somnifera*) (×40) showing mild hyalinization, no glomerular destruction, and no necrosis. **h** Treated group (Ag NPs 100 nm with *W. somnifera*) (×40) showing normal kidney architecture and glomerula. **i** Treated group (rod 100-nm Ag NPs with *W. somnifera*) (×40) showing normal kidney architecture and glomerula

mild hyalinization, eosinophilia, and mild glomerular destruction (Fig. 7a–c.) Spherical 100 nm and rod-shaped 100-nm Ag NPs showed normal glomerula and mild hyalinization (Fig. 7d, e). *W. somnifera* significantly normalized the

changes with 20-nm Ag NPs and 50-nm Ag NPs, resulting in mild to negligible hyalinization, eosinophilia, glomerular destruction, and necrosis for both (Fig. 7f, g). *W. somnifera* with 100-nm spherical-shaped and 100-nm rod-shaped Ag NPs showed normal kidney architecture, glomerula, and cells (Fig. 7h, i).

Discussion

Ag NPs have been used in health implications as anti-microbial agents and disinfectants for a very long time (Choi et al. 2009). As information presented in the literature, different sizes and shapes of Ag NPs have different toxic effects (Edwards-Jones 2009; Nel et al. 2006). In the present study, a comparison was done between different sizes and shapes of Ag NPs for their acute oral toxicity (Park and Bae 2010) for their potential application as anti-microbial agents, and acute toxicity modulation by *W. somnifera* was observed. In a previous study, bare Ag NPs (42 nm) in distilled water with doses of 0.25, 0.5, and 1 mg/kg induce hepatotoxicity by repeated oral administration (Kim et al. 2009; Oberdorster et al. 2005). Particle morphology plays a significant role in the toxicology of various kinds of nanoparticles (Larissa et al. 2011; Sharma 2010).

The absorbance spectroscopy data of Ag NP solution was explored, and a comparison between various sizes and shapes of Ag NPs investigated single peaks for 20, 50, and 100 nm spherical-shaped Ag NPs at different wavelengths and two peaks for 100-nm rod-shaped Ag NPs due to the distribution of radii and orientation of the particles in the solution, respectively.

The different sizes and shapes of nanoparticles can produce different biological responses and severe toxicity to tissue causing cell injury (Lam et al. 2004). Many studies suggested that crystalline small particles can induce more toxic to cells as well as being more persistent in the tissues (Linda et al. 2011). In this study, various sizes and shapes of Ag NPs produce different cell viability in macrophages. From the results obtained, it appears that 100-nm spherical- and rod-shaped Ag NPs caused no significant change, while at 20- and 50-nm spherical shapes of Ag NPs, there is a significant increase in plasma SGOT, SGPT, and ALP activities. The elevated levels of SGOT, SGPT, and ALP indicated a diseased level. SGPT and SGOT both are the liver-specific enzymes and used to diagnose liver diseases (Yong et al. 2010; Yadav et al. 2013; Shayestech et al. 2014). The studies showed that silver disrupts the activity of mitochondria, and this causes a rise in plasma transaminase (GOT, GPT) activity which is a sensitive indicator of damage to cytoplasmic and/or mitochondrial membranes (Oberdorster et al. 2005; Fabian et al. 2013). Slight effect of BUN and creatinine concentration was measured. Acute oral toxicity was also confirmed by histopathological changes in liver and kidney tissues that revealed marked mononuclear cell infiltration, nuclear degeneration, architectural disarray, glomerular destruction, and necrosis. On the other hand, the associated anatomy of these structures causes the damage of a part leading to disruption of the other parts (Yadav et al. 2013; Fabian et al. 2013; Singh et al. 2001).

Spherical-shaped Ag NPs increased glomerular destruction, and central vein and portal triad destruction causes severe hepatorenal toxicity. Hepatorenal and renal toxicity of Ag NPs was reduced significantly when the rats were treated with *W. somnifera* in the present case which indicated that *W. somnifera* has free radical scavenging enzymes that worked as anti-oxidant and normalizes all enzymatic activities and improves BUN and creatinine concentration. *W. somnifera* should be used and worked further as a toxicity modulator.

Conclusion

It is demonstrated that Ag NPs show toxicity in macrophages and Wistar rats. The toxicity of spherical-shaped Ag NPs is inversely proportional to their size which is due to deeper and higher penetration of small-sized nanoparticles; 100-nm rod-shaped Ag NPs showed negligible toxicity in comparison to 100-nm spherical-shaped nanoparticles in macrophages under in vitro conditions and in Wistar rats. When Ag NPs of different shapes and sizes were treated with extracts of *W. somnifera* administered to rats, the toxic effects were found to be reduced to a significant extent. This study indicates the potential use of *W. somnifera* extract as an anti-oxidant and anti-inflammatory against the toxic effects of different shapes and sizes of Ag NPs. The prospective applications *W. somnifera* will necessitate significant consideration by scientific community in the future.

Acknowledgments Authors are thankful to Dr. G. N. Qazi, Vice Chancellor, Jamia Hamdard, New Delhi, for providing working facilities. Authors are also grateful to the Department of Science and Technology (DST), Government of India, for financial support.

Conflict of interests The author(s) declare that they have no competing interests.

Authors' contributions Ag NPs were synthesized, characterized, and studied in vivo by MFA and DY. Statistical analyses were done by MFA, DY, RKK, JC, SR, IA, and MS that were involved in the inception and planning of the project and in the preparation of the manuscript. All authors read and approved the final manuscript.

References

Abou-Douh AM (2002) New withanolides and other constituents from the fruit of *Withania somnifera*. Arch Pharm 335:267–276

Ahamed M, Alsalhi MS, Siddiqui MKJ (2010) Silver nanoparticle applications and human health. Clin Chim Acta 411:1841

Alarco EI, Udekwu K, Skog M et al (2012) The biocompatibility and antibacterial properties of collagen-stabilized photochemically prepared silver nanoparticles. Biomaterials 33:4947

Allain CC, Poon LS, Chan CSG et al (1978) Enzymatic determination of total serum urea. Clin Chem 20:470–475

Anwar MF, Yadav D, Kapoor S et al (2013) Comparison of antibacterial activity of Ag nanoparticles synthesized from leaf extract of *Parthenium hystrophorus* L in aqueous media and gentamicin sulphate: in-vitro. Drug Dev Ind Pharm. doi:10.3109/03639045.2013.845840

Bhattacharya A, Ghosal S, Bhattacharya SK (2001) Anti-oxidant effect of *Withania somnifera* glycol withanolides in chronic foot shock stress-induced perturbations of oxidative free radical scavenging enzymes and lipid peroxidation in rat frontal cortex and striatum. J Ethno Pharmacol 74:1–6

Budhiraja RD, Sudhir S, Garg KN et al (1987) BC: review of biological activity of withanolides. J Sci Ind Res 46:488–491

Carlson C, Hussain SM, Schrand AM et al (2008) Unique cellular interaction of silver nanoparticles: size-dependent generation of reactive oxygen species. The J Physic Chem B 112:13608–13619

Chaudhary G, Sharma U, Jagannathan NR et al (2003) Evaluation of *Withania somnifera* in a middle cerebral artery occlusion model of stroke in rats. Clin Exp Pharmacol Physiol 30:399–404

Cheng D, Yang J, Zhao Y (2004) Antibacterial materials of silver nanoparticles application in medical appliances and appliances for daily use. Chin Med Equip J 4:26–32

Choi O, Clevenger TE, Deng B et al (2009) Role of sulfide and ligand strength in controlling nanosilver toxicity. Water Res 43:1879–1886

Cohen MS, Stern JM, Vanni AJ et al (2007) In vitro analysis of a nanocrystalline silver-coated surgical mesh. Surg Infect 8:397–403

Dhalla NS, Sastry NS, Malhotra CL (1961) Chemical studies of the *Withania somnifera*. J Pharm Sci 50:876–877

Edwards-Jones V (2009) The benefits of silver in hygiene, personal care and health care. Lett Appl Microbiol 49:147–152

Fabian H, Martin JD, Rothen-Rutishauser CB et al (2013) Exposure of silver-nanoparticles and silver-ions to lung cells in vitro at the air-liquid interface. Part Fibre Toxicol 10:11

He BL, Tanm JJ, Kong YL et al (2004) Synthesis of size controlled Ag nanoparticles. J Mol Catal A: Chem 221:121–126

Huiliang C, Xuanyong L, Fanhao M et al (2011) Biological actions of silver nanoparticles embedded in titanium controlled by micro-galvanic effects. Biomaterials 32:693–705

Husdan H, Rapoport A (1968) Estimation of creatinine by the Jaffe reaction: a comparison of three methods. Clin Chem 14:222–238

Kandil FE, Elsayeh NH, Abou-Douh AM et al (1994) Flavonol glycosides and phenolics from *Withania somnifera*. Phytochemistry 37:1215–1216

Kim WY, Kim J, Park JD et al (2009) Histological study of gender differences in accumulation of silver nanoparticles in kidneys of Fischer 344 rats. J Toxicol Environ Health A 72:1279–84

King PRM, King EJ (1954) Estimation of plasma phosphatase by determination of hydrolysed phenol with amino-antipyrene. J Clin Path 7:322–326

Kulkarni RR, Patki PS, Jog VP et al (1991) Treatment of osteoarthritis with a herbomineral formulation: a double-blind, placebo-controlled, cross-over study. J Ethnopharmacol 33:91–95

Kumar OA, Jyothirmayee G, Tata SS (2011) In vitro plant regeneration from leaf explants of *Withania somnifera* (L) Dunal (Ashwaganda)—an important medicinal plant. Res Biotech 2:34–3

Lam PK, Chan ES, Ho WS et al (2004) In vitro cytotoxicity testing of a nanocrystalline silver dressing (Acticoat) on cultured keratinocytes. Br J Biomed Sci 61:125–127

Lankveld DP, Oomen AG, Krystek P et al (2010) The kinetics of the tissue distribution of silver nanoparticles of different sizes. Biomaterials 31:8350–8361

Lansdown A (2006) Silver in health care: antimicrobial effects and safety in use. Curr Probl Dermatol 33:17–34

Larissa VS, Andrea AD, Jong SK et al (2011) Nanosilver induces minimal lung toxicity or inflammation in a subacute murine inhalation model. Part Fibre Toxicol 8:5

Linda CS, Edgar G, Andreas S et al (2011) Shape matters: effects of silver nanospheres and wires on human alveolar epithelial cells. Part Fibre Toxicol 8:36

Liu L, Yang J, Xie J et al (2013) The potent antimicrobial properties of cell penetrating peptide-conjugated silver nanoparticles with excellent selectivity for gram-positive bacteria over erythrocytes. Nanoscale 5:3834–40

Lu W, Senapati D, Wang S et al (2010) Effect of surface coating on the toxicity of silver nanomaterials on human skin keratinocytes. Chem Phys Lett 487:92

Muangman P, Chuntrasakul C, Silthram S et al (2006) Comparison of efficacy of 1% silver sulfadiazine and Acticoat for treatment of partial-thickness burn wounds. J Med Assoc Thai 89:953–958

Nel A, Xia T, Madler L et al (2006) Toxic potential of materials at the nanolevel. Science 311:622–627

Nel A, Xia T, Meng H et al (2012) Nanomaterial toxicity testing in the 21st century: use of a predictive toxicological approach and high throughput screening. Acc Chemi Res. doi:10.1021/ar300022h

Nittala SS, Lavie S (1988) Chemistry and genetics of withanolides in *Withania somnifera* hybrids. Phytochemistry 20:2741–2748

Niyaz A, Siddiqui EN (2014) Seed germination of *Withania somnifera* (L.) Dunal. Eur J Med Plants 4:920–926

Oberdorster G, Maynard A, Donaldson K et al (2005) Principles for characterizing the potential human health effects from exposure to nanomaterials: elements of a screening strategy. Part Fibre Toxicol 2:8

Oberpichler H, Sauer D, Rossberg C et al (1990) PAF antagonist ginkgolide B reduces postischemic neuronal damage in rat brain hippocampus. J Cereb Blood Flow Metab 10:133

Panda S, Kar A (1997) Evidence for free radical scavenging activity of Ashwagandha root powder in mice. Ind J Physio Pharmaco 41:424–426

Park E, Bae E (2010) Repeated-dose toxicity and inflammatory responses in mice by oral administration of silver nanoparticles. Environ Toxicol Pharm 30:162–168

Park J, Lim DH, Lim HJ et al (2011) Size dependent macrophage responses and toxicological effects of Ag nanoparticles. Chem Commun 47:4382

Reitman S, Frankel S (1957) Glutamic—pyruvate transaminase assay by colorimetric method. Am J Clin Path 28:56

Sharma M (2010) Understanding the mechanism of toxicity of carbon nanoparticles in humans in the new millennium: a systemic review. Indian J Occup Environ Med 14:3–5

Sharma V, Sharma S, Pracheta et al (2011) *Withania somniforma*: a rejuvinating Ayurvedic medicinal herb for the treatment of various human ailments. Intl J Pharm Tech Res 3:187–192

Shayestech TH, Khajavi F, Ghasemi H et al (2014) Effects of silver nanoparticle (Ag NP) on oxidative stress, liver function in rat: hepatotoxic or hepatoprotective? Issues Biol Sci Pharma Res 2:40–44

Singh B, Saxena AK, Chandan BK et al (2001) Hepatoprotective activity of indigtone—a bioactive fraction from *Indigo feratinctoria* Linn. Phytother Res 15:294–7

Singh B, Chandan BK, Gupta DK (2003) Adaptogenic activity of a novel withanolide-free aqueous fraction from the roots of *Withania somnifera* Dun. (Part II). Phytother Res 17:531–6

Wagner H, Norr H, Winterhoff H (1994) Plantadaptogens. Phytomedicine 1:63–76

Wang H, Qiao X, Chen J, Ding S (2005) Preparation of silver nanoparticles by chemical reduction method. Coll Surf A Physico Chem Eng Asp 256:111–115

Wilhelm M, Zhao CL, Wang Y et al (1991) Poly(styrene-ethylene oxide) block copolymer micelle formation in water: a fluorescence probe study. Macromolecules 24:1033–1040

Yadav D, Chaudhary AA, Garg V et al (2013) In vitro toxicity and antidiabetic activity of a newly developed polyherbal formulation (MAC-ST/001) in streptozotocin-induced diabetic Wistar rats. Protoplasma 250:741–749

Yong SK, Moon YS, Jung DP et al (2010) Subchronic oral toxicity of silver nanoparticles. Part Fibre Toxicol 7:20

Zhang Y, Sun J (2007) A study on the bio-safety for nano-silver as antibacterial materials. Chin J Med Instrum 31:35–38